Author accepted manuscript version of the publication in
IEEE Transactions on Nuclear Science, volume 70, issue 4, April 2023.
Published version: https://doi.org/10.1109/TNS.2023.3242267

Charge Collection in SOI Microdosimeters and Their Radiation Hardness

V. A. Pan, *Student Member, IEEE*, L. T. Tran, *Member, IEEE*, Z. Pastuovic, D. Hill, J. Williams, A. Kok, M. Povoli, A. Pogossov, S. Peracchi, D. Boardman, J. Davis, S. Guatelli, M. Petasecca, M. L. F. Lerch, *Member, IEEE*, and A. B. Rosenfeld, *Life Senior Member, IEEE*

***Abstract*— A new batch of microdosimeters has been extensively studied for their charge collection efficiency (CCE) properties, as well as their radiation hardness for medical, space and accident applications. Silicon-on-insulator (SOI) microdosimeters with an active layer thickness of 10, 20, and 50 μm have been investigated and were characterized with a 24 MeV carbon ion beam as well as a Co-60 gamma source. A negative pulse was observed in addition to the positive pulses generated within the sensitive volumes (SVs) by incident ions which led to undesirable low energy events in the SOI microdosimeters response. To study this phenomenon, the microdosimeters were irradiated with gamma radiation from a Co-60 source with a total dose of 3 and 10 Mrad(Si). It was determined that the negative pulse was originating from the support wafer due to the displacement current phenomenon. Irradiation with the Co-60 source led to a disappearance of the negative pulse due to an increase in recombination within the support wafer while almost no changes in CCE were observed. A radiation hardness study was also performed on the 50 μm SOI microdosimeter with 16 SVs being irradiated with a fluence of $\sim 10^8$ ^{12}C ions/cm^2. A CCE deficit of approximately 2% was observed at an operation bias of 10 V within the SVs. The findings of this work demonstrate that the SOI microdosimeters can be utilized in space and medical applications as they can handle typical levels of dose encountered in these applications. Additionally, evidence for SOI microdosimeter fabrication standards in terms of support wafer resistivity and buried oxide (BOX) thickness is shown.**

***Index Terms*— Microdosimeter, radiation damage, radiation hardness, silicon-on-insulator (SOI).**

I. Introduction

SILICON-ON-INSULATOR (SOI) microdosimetry has become a valuable tool in particle therapy for relative biological effectiveness (RBE) prediction as well as dose averaged linear energy transfer (LET_D) verification [1]. It has also been proven to be useful in shielding evaluation for space travel when encountering radiation typical to galactic cosmic rays (GCRs) [2]. SOI microdosimeters possess the capability to measure a large range of LET(Si) thus making it suitable for single event upset (SEU) prediction including neutron fields in which the boron neutron capture (BNC) reaction releases an alpha and lithium ion [3]. When these applications are studied for extended periods of time with single devices, the intense hadronic radiation field generally leads to a degradation of the device through damage to the bulk silicon as well as the field oxide above the SOI active layer. Damage from hadronic interactions to the device includes increased leakage current, a change in the resistivity of the active layer as well as a decrease in charge collection efficiency (CCE) [4], thus an understanding of the radiation hardness of SOI microdosimeters is of great interest for a wide range of applications including the medical physics (particularly for quality assurance (QA) in particle therapy), space communities to understand the life span and working limits of the detectors during a Moon or Mars mission, as well as accident applications, e.g., a reactor meltdown where it is important to measure a low or moderate flux of thermal neutrons in the presence of a huge gamma component.

The two types of radiation damage explored in this work are total ionizing dose (TID) [5] and displacement damage (DD) [6] associated with ionizing energy losses (IEL) and Non-IEL (NIEL), respectively. High energy photons and charged particles that interact with electronic devices create electron hole pairs in the silicon oxide that may not recombine and are potentially left as free carriers and form trapped charges [7]. This is referred to as the TID effect. When a high energy particle (protons, electrons, neutrons, heavy ions) interacts with an electronic device, it can potentially displace the atoms of the device as it passes through [6]. If an atom is displaced, the vacancies and interstitials created allow for new energy states in the band gap of the semiconductor which causes changes in the performance of the device. This is referred to as the DD effect.

The current gold standard for microdosimetric measurements is the tissue equivalent proportional counter (TEPC). The downsides of this detector are that it is bulky in size, has a limited spatial resolution and requires a very high operational voltage. This poses several limitations [8] specifically for particle therapy application for RBE evaluation, where high spatial resolution is essential specifically at the distal parts of

Manuscript received 20 December 2022; revised 25 January 2023 and 31 January 2023; accepted 1 February 2023. Date of publication 3 February 2023; date of current version 18 April 2023. This work was supported in part by the Australian Research Council under Grant DP170102273 and in part by the European Space Agency (ESA) Technology Research Program (TRP) under Contract 4000133574/21/NL/CRS.

V. A. Pan, L. T. Tran, D. Hill, J. Williams, A. Pogossov, S. Guatelli, M. Petasecca, M. L. F. Lerch, and A. B. Rosenfeld are with the Center of Medical and Radiation Physics, University of Wollongong, Wollongong, NSW 2522, Australia (e-mail: vp881@uowmail.edu.au; tltran@uow.edu.au; dbh522@uowmail.edu.au; jw734@uowmail.edu.au; apogosso@uow.edu.au; susanna@uow.edu.au; marcop@uow.edu.au; mlerch@uow.edu.au; anatoly@uow.edu.au).

Z. Pastuovic, S. Peracchi, D. Boardman, and J. Davis are with the Australian Nuclear Science and Technology Organization (ANSTO), Lucas Heights, NSW 2234, Australia (e-mail: zkp@ansto.gov.au; speracch@ansto.gov.au; dbn@ansto.gov.au; jbd@ansto.gov.au).

A. Kok and M. Povoli are with SINTEF, 0314 Oslo, Norway (e-mail: angela.kok@sintef.no; marco.povoli@sintef.no).

Color versions of one or more figures in this article are available at https://doi.org/10.1109/TNS.2023.3242267.

the Bragg peak (BP). The use of TEPC's for characterization of the quality of space radiation fields and dose equivalent derivation on the International Space Station (ISS) has been demonstrated, however its application in spacecrafts is limited due to aforementioned shortcomings, along with observed pulse pile up effects during a solar particle event (SPE) burst [9].

The Center for Medical and Radiation Physics (CMRP), Wollongong, Australia, has been involved in the successful designing and development of 3-D SOI microdosimeters for over two decades. A new batch of devices has recently been fabricated at SINTEF, Norway, on SOI wafers which include a matrix of 40 × 40 cylindrical sensitive volumes (SVs) of varying thickness – 10, 20, and 50 μm and a 20 μm diameter with odd and even rows of linear arrays of SVs which can be readout independently. These devices have a trenched planar structure [10] and their fabrication process has been described elsewhere [11]. The devices have an active area of 2 × 2 mm^2 which is mounted onto a dual-in-line (DIL) 20 package. This device batch is referred to as the PBS full mushroom microdosimeters.

Previous generations of the SOI microdosimeters have been extensively characterized [3], [12] and applied in a variety of studies. These include space and aviation studies [2], [13], [14], [15], low dose rate radon studies [16], RBE and LET$_D$ verification [1], [10], [17], [18], cell survival studies [19] as well as studies with low energy ions with very high LET [20]. In addition, other groups have reported success with SOI technology in hadron therapy [21], [22]. To further improve results gathered in patient treatment planning in scanning beams as well as in low dose rate space radiation environments, it is critical to continue improving the design and functionality of the devices based on previous experiences. Various thicknesses of the SV are critical in evaluating various regions of the BP, with thicker devices being suitable for assessing the lower LET component, while thinner devices are required for higher LET measurements at the distal edge of the BP.

In this work, we study the response of our new batch of SOI microdosimeters to a large gamma dose (TID effect) utilizing a Co-60 gamma irradiation as well as the performance after irradiation with 24 MeV carbon ions (DD effect). The aim of this work is to show that the SOI microdosimeters can withstand the typical fluence and doses that are expected in medical QA and space applications. Additionally, the origin of an unexpected negative pulse is also studied that is present only in the devices with a 10 and 20 μm device layer when irradiated with 24 MeV carbon ions.

II. Materials and Methods

A. 3-D SOI Microdosimeter

1) PBS Full Mushroom Microdosimeter: The PBS full mushroom microdosimeters (shown in Fig. 1) were fabricated on SOI wafers with 10, 20, and 50 μm thick active layer with a trenched planar structure (i.e., the n+ core region was produced by ion implantation and the p+ cylindrical wall surrounding the SV was produced by deep reactive ion etching followed by filling in with polysilicon and boron diffusion [11]). In this device batch the 500 μm thick p-type silicon support wafer has a resistivity of 1-30 Ωcm while the device layer [above the buried oxide (BOX)] has a resistivity of >5 kΩcm.

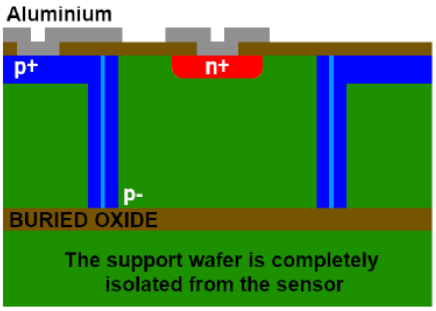

Fig. 1. Schematic of the SOI PBS full mushroom microdosimeter SV structure.

B. MicroPlus (μ^+) Probe

Two in house built MicroPlus (μ^+) probes [18] were utilized for the readout of the microdosimeters. Devices with an active layer of 10 μm utilized a probe with an 8 MeV dynamic range while detectors with an active layer thickness of 20 and 50 μm used a probe with a 40 MeV dynamic range. Due to the different probes being utilized, a different noise level threshold was set for each of the two probes. The low level discriminator (LLD) for the 8 and 40 MeV μ^+ probes were then set to ∼90 and ∼1300 keV, respectively.

C. Irradiation Facilities

1) Ion Beam Induced Charge Collection (IBIC) Study at SIRIUS Accelerator Beamline at ANSTO, Australia: The CCE of the new mushroom microdosimeters was studied using an IBIC technique at the 6 MV SIRIUS accelerator located at the Center for accelerator sciences (CAS) facility at the Australian Nuclear Sciences and Technology Organization (ANSTO). This system includes a Confocal Heavy Ion MicroProbe (CHIMP) which was used to deliver carbon ions at an energy of 24 MeV with a range of approximately 27 μm in Si and a microbeam diameter of 1.2–1.5 μm. The devices were raster scanned over a wide range of scan sizes at a beam rate of approximately 1 kHz. The x and y position of the microbeam as well as the deposited energy (E) for each event was recorded and processed into a list mode file allowing for median energy maps to be generated. Fig. 2 shows the SOI microdosimeter inside of the SIRIUS vacuum chamber at ANSTO. The microdosimeter is mounted on a specially designed circuit board which is then connected by short wires to the low noise front-end MicroPlus probe. The probe is then connected through the chamber to the shaping amplifier and ADC which are outside of the vacuum chamber.

2) Gamma Irradiation at the Gamma Technology Research Irradiator (GATRI) at ANSTO: In order to understand the radiation hardness of the mushroom microdosimeters, the devices were irradiated by a Co-60 source at the GATRI at ANSTO with 3 or 10 Mrad(Si) (30 and 100 kGy) with a dose rate of 0.62 kGy/h. During irradiation, each device was wrapped

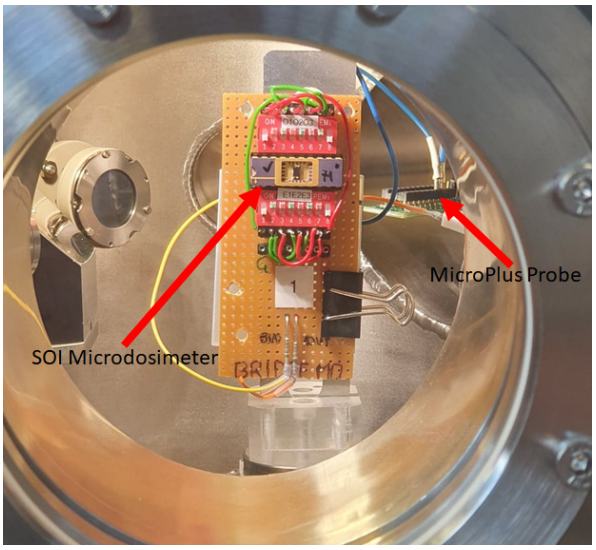

Fig. 2. Experimental set up inside of the vacuum chamber of the SIRIUS beamline at ANSTO to perform CCE studies with the microdosimeters.

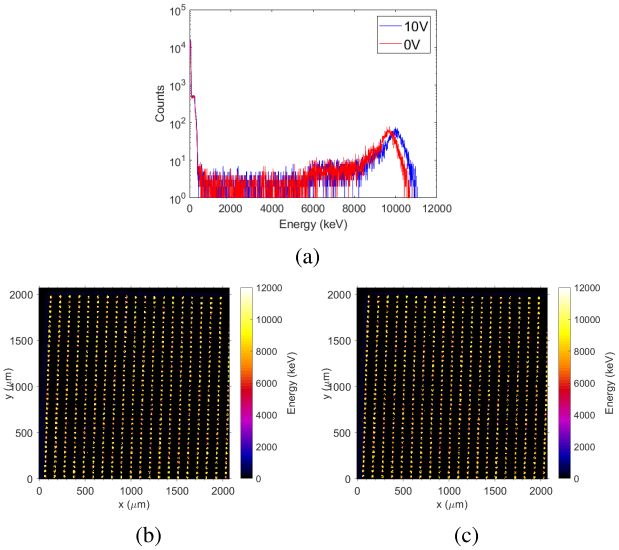

Fig. 3. (a) MCA spectra of the 10 μm mushroom PBS full after irradiation with a 24 MeV ^{12}C ion scanning microbeam across the SV region along with the corresponding median energy maps for (b) 0 and (c) 10 V.

in a thin 10 μm aluminum foil in order to avoid electrostatic charge build up which could lead to breakdown of the device. Two weeks after irradiation with the Co-60 source, the devices were then further tested utilizing the IBIC technique.

III. Results and Discussion

A. 10 μm PBS Full Microdosimeter

Fig. 3 shows a zoomed out median energy map of the 10 μm mushroom PBS full showing the SV region at 0 and 10 V (Fig. 3(b) and (c), respectively) with both the odd and even array biased, along with the corresponding MCA spectra [Fig. 3(a)]. There exists a clear shift to a higher energy for the 10 V MCA spectra versus the 0 V spectra. This is expected as the microdosimeter is at full depletion under a 10 V bias allowing for better overall CCE. Such results are consistent with previous studies [20]. The primary peak at 8–11 MeV is related to the energy deposited within the

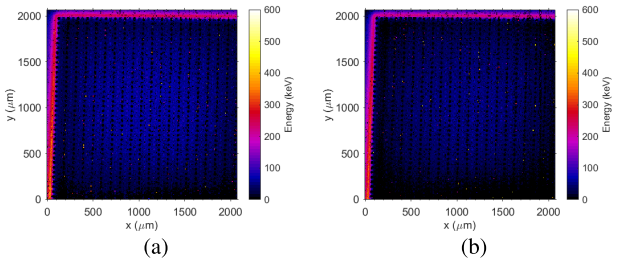

Fig. 4. 10 μm mushroom PBS full at (a) 0 and (b) 10 V showing only the 0–600 keV region.

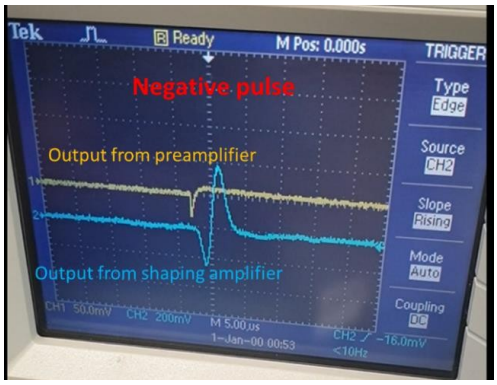

Fig. 5. Negative pulse as observed by the oscilloscope.

SV by the carbon ion beam. This value of deposited energy is consistent with expectation based on SRIM [23], which predicts the maximum LET for 24 MeV carbon ions to be approximately 1190 keV/μm in silicon, meaning that in this microdosimeter, we expect ~11.9 MeV to be deposited. The low energy peak present at 0–600 keV energy region is not expected. Although the median energy map images appear to show nothing out of the expected charge collection, upon further inspection, by creating a separate 0–600 keV energy window for 0 and 10 V (Fig. 4(a) and (b), respectively), it is observed that there exists a low energy halo within the region between SVs. As can be observed, this halo is present at both 0 and 10 V without any major differences. The MCA spectra also show no significant differences between 0 and 10 V bias. A detailed analysis of these events demonstrated that they are corresponding to the positive overshooting of a negative pulse from the charge sensitive preamplifier while events within the SV produce positive pulses as was observed with the cathode ray oscilloscope (CRO) (Fig. 5). Fig. 6 shows the median energy map of the 10 μm mushroom device at 10 V after a 3 Mrad(Si) Co-60 irradiation in which it is clearly seen that the low energy events from the negative pulse overshoot have disappeared. The corresponding MCA spectra shown in Fig. 6(a) demonstrates that the low energy shoulder present before the 3 Mrad(Si) irradiation at ~300 keV has disappeared after the Co-60 irradiation. It is also evident that there is a ~10% loss of CCE within the SV, as the high energy edge of the full energy peak shifts from ~11 MeV down to 10 MeV. The observed negative pulses that were opposite polarity and higher amplitude on the output of the charge sensitive preamplifier in comparison to the expected pulse amplitude associated with the deposited energy by 24 MeV carbon ions in the SV of the 10 μm

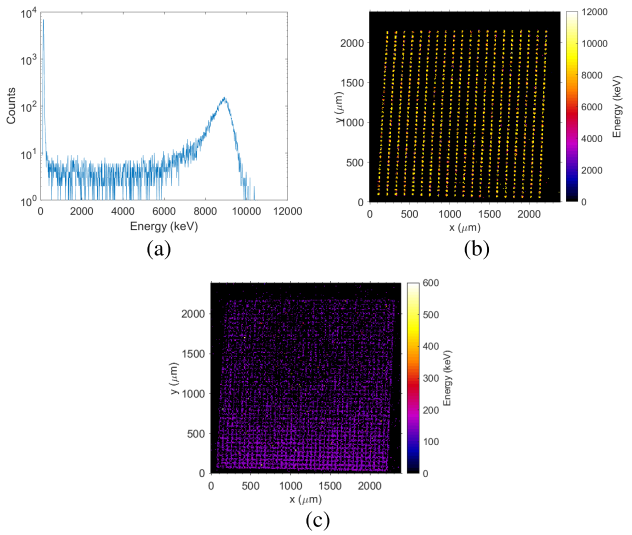

Fig. 6. (a) MCA spectra of the 10 μm mushroom PBS full after the 3 Mrad(Si) Co-60 irradiation with (b) full median energy map and (c) 0–600 keV region.

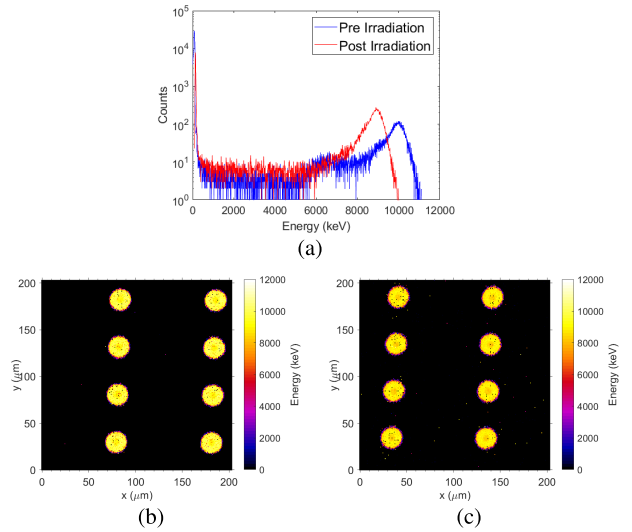

Fig. 7. MCA spectra and (a) median energy map of the 10 μm mushroom PBS full (b) before the 10 Mrad(Si) Co-60 irradiation and (c) after the irradiation.

mushroom device can be explained by energy deposition by the ion within the support wafer. This is further confirmed by the absence of a negative pulse presence in the 50 μm mushroom device (as will be demonstrated later) due to the lower range of the ion, thus not penetrating into the support wafer. The nature of the negative pulses can be explained by the displacement current observed in the MOS SOI capacitor due to the change in potential at the Si/SiO_2 interface when an ion incident between SVs produces a plasma track in the BOX and support wafer that leads to collected charge that is larger than expected from the SV of the SOI device due to a higher residual energy being released in the 500 μm support wafer in comparison to the energy deposited into the SV [24]. These negative pulses have not been observed in previous batches of microdosimeters due to lower resistivity of the support wafer (about 0.01 Ωcm in contrast to typical 30 Ωcm) and a thicker BOX (2 μm in contrast to 0.6 μm in this batch).

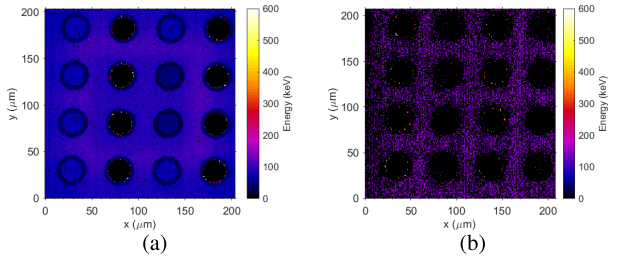

Fig. 8. 0–600 keV energy region of the 10 μm mushroom PBS full (a) before and (b) after the 10 Mrad(Si) Co-60 irradiation with the odd array connected to the MicroPlus while the even array is floating [first and third row in Fig. 8(a) and second and fourth row in Fig. 8(b)].

Schwank et al. [24] demonstrated a strong dependence of the excess charge collection due to displacement current on the resistivity and BOX thickness showing a significant increase in current with a thinner BOX and higher substrate resistivity. Irradiations with 3 Mrad(Si) gammas essentially reduces the carrier life time within the supporting wafer minimizing the displacement current by allowing for faster recombination of e–h pairs in the ion plasma track.

Fig. 7 shows the MCA spectra [Fig. 7(a)] and the zoomed in median energy map for the 10 μm mushroom PBS full before [Fig. 7(b)] and after [Fig. 7(c)] a 10 Mrad(Si) gamma irradiation. Deficit observed in the charge collection of the microdosimeter is almost identical as after the 3 Mrad(Si) dose (Fig. 6), suggesting that the TID above 3 Mrad(Si) does not further reduce the life time of the minority charge carriers in the SV. The 0–600 keV windowed median energy map (Fig. 8) shows that most of the uniformly distributed low energy events with an energy of $\sim$100 keV [corresponding to a blue color coding in Fig. 8(a)] occurring between the SVs and in the SVs (only the odd array was read-out while the even array was floating) had disappeared after irradiation [Fig. 8(b)]. This was confirmed by an absence of the negative pulse which produced a positive overshoot. However now, another set of low energy events [at approximately 200 keV corresponding to the violet color coding in Fig. 8(b)] are uniformly distributed between the SVs. These events originate due to energy deposition by the carbon ions in the device layer when incident between the SVs. It is obvious that these events are absent when the ion is incident within the SV. The origin of these events is addressed in Section III-B.

B. 20 μm PBS Full Microdosimeter

Fig. 9(a) shows the MCA spectra of the 20 μm PBS full microdosimeter before and after a 10 Mrad(Si) gamma irradiation. There is an evident shift in the full energy peak after the 10 Mrad(Si) gamma irradiation corresponding to a $<$2% decrease in CCE. There is also a significant increase in low energy events corresponding to charge collection between the SVs. Fig. 9(b) and (c) shows a zoomed in median energy map of the microdosimeter before and after a 10 Mrad(Si) gamma irradiation, respectively. Fig. 9(d) shows the zoomed in median energy map corresponding to the energy window of 0–3000 keV after a 10 Mrad(Si) irradiation. It is obvious that events with an energy of about 1500 keV are uniformly distributed between the SVs. Note, all images are shown at

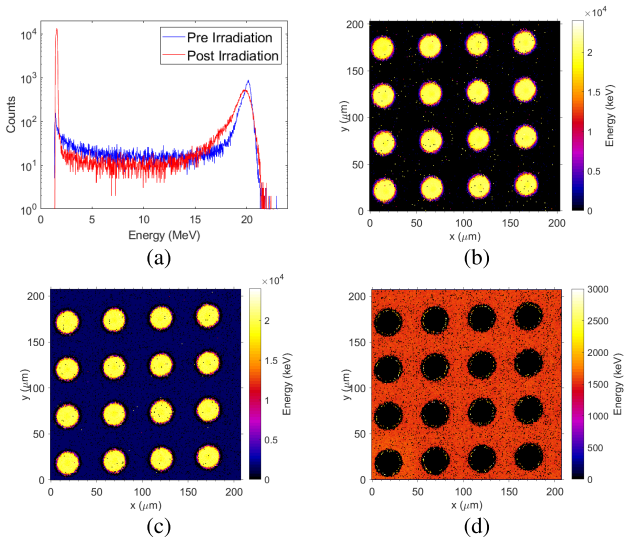

Fig. 9. (a) MCA spectra before and after a 10 Mrad(Si) gamma irradiation for the 20 μm mushroom PBS full at 10 V and the corresponding median energy map for (b) 16 SVs before, (c) 16 SVs after the 10 Mrad(Si) gamma irradiation, and (d) 0–3000 keV energy window after a 10 Mrad(Si) gamma irradiation.

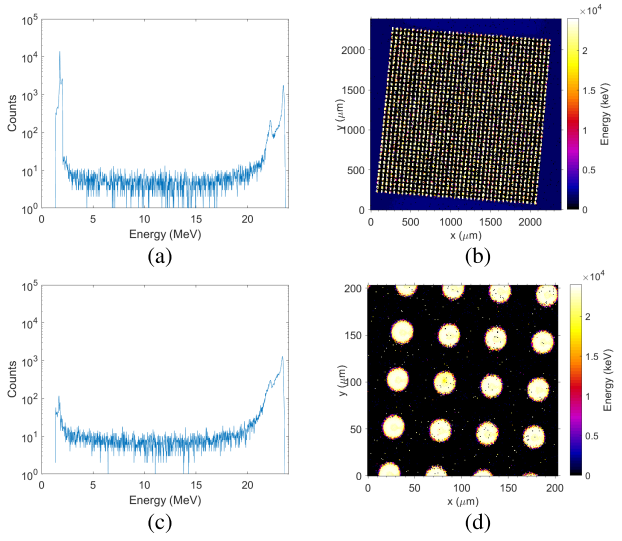

Fig. 10. (a) MCA spectra, (b) median energy map of 50 μm mushroom PBS full at 10 V for the entire device, (c) MCA, and (d) median energy map of 16 SVs before the 10 Mrad(Si) irradiation with Co-60.

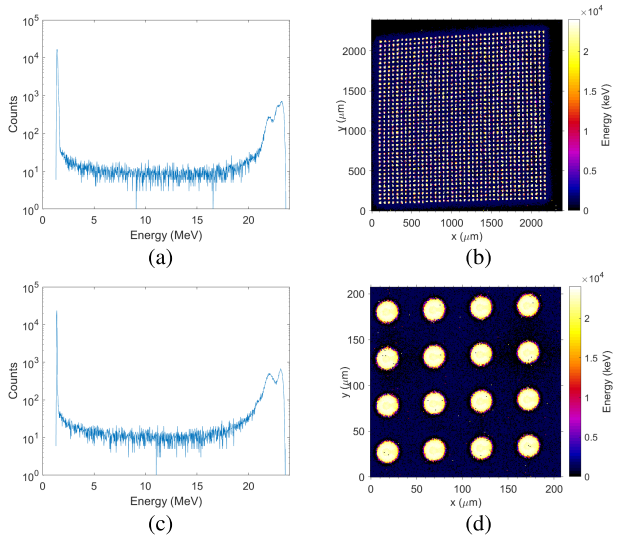

Fig. 11. (a) MCA spectra, (b) median energy map of 50 μm mushroom PBS full at 10 V for the entire device, (c) MCA, and (d) median energy map of 16 SVs after the 10 Mrad(Si) irradiation with Co-60.

a 10 V bias on both the odd and even arrays. The nature of these events is associated with a positive buildup of charge in the field oxide produced by the gamma irradiation leading to an inverse n+ layer under the field oxide between the SVs. The inverse n+ layer and p-Si device layer produce a p-n-junction in which charge generated by incident ^{12}C ions is collected by diffusion with enhanced charge collection in the region adjacent to the p+ electrode of the SV that is reflected in the rings with increased CCE within the SVs in Fig. 9(d). It is clear that an increase in the thickness of the device layer leads to an increase in the energy of these events present between the SVs due to a more pronounced charge collected by diffusion from the high resistivity p-Si device layer. Fig. 8(b) shows that these events arise at approximated 200 keV for the 10 μm SOI active layer and Fig. 9(d) show that the events are at approximately 1500 keV for the 20 μm SOI active layer. A detailed quantitative analysis requires accurate knowledge of the initial resistivity and life time of the charge carriers of the 10 and 20 μm thick high resistivity p-Si device layers which are at this stage unknown.

C. 50 μm PBS Full Microdosimeter

Fig. 10 shows the median energy map and corresponding MCA spectra for the 50 μm mushroom PBS full microdosimeter at a bias of 10 V as well as a zoomed in image of 16 SVs before a 10 Mrad(Si) irradiation. It is observed that there exists no events from the positive overshoot of the negative pulse above the LLD of 1 MeV within this device. This is due to the range of the 24 MeV carbon ion beam being smaller than the active layer thickness so no energy is deposited by the ^{12}C ion into the substrate to generate the aforementioned negative pulses. However, it is seen that there exists low energy events at approximately 2 MeV which are coming from outside of the matrix of SVs. The MCA spectra shows that the carbon ions stop within the SV–this is clear as there is a sharp fall off from the main energy peak at ~24 MeV. The second lower energy peak present near the full energy peak corresponds to the ions incident on the Al bus and entering the SV with lower energy and greater straggling which is reflected in a wider peak.

After a 10 Mrad(Si) irradiation with Co-60, the low energy events outside the SV matrix are observed to disappear above the LLD of 1 MeV [as shown in Fig. 11(b)] however there are now observed low energy events between the SVs as a consequence of the irradiation due to buildup of positive charge in the field oxide which has been described in the earlier sections and is clearly shown from the comparison of the MCA spectra in Figs. 10(c) and 11(c) and the median energy maps in Figs. 10(d) and 11(d).

D. Radiation Hardness Study With Carbon Ions

Following the 10 Mrad(Si) gamma irradiation, the 50 μm PBS full mushroom microdosimeter was irradiated

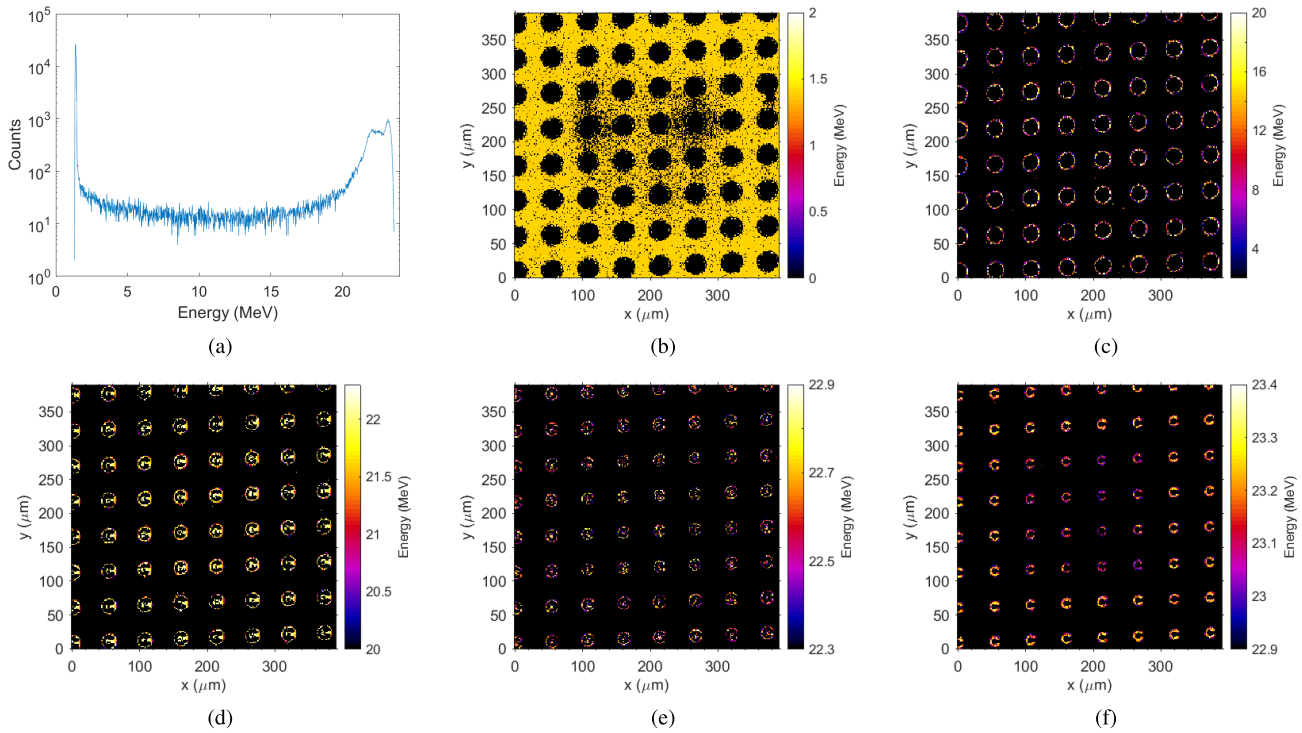

Fig. 12. (a) MCA spectra of the 50 μm mushroom PBS full at 10 V after 16 SVs were irradiated with an approximate ^{12}C ion fluence of 10^8 cm^{-2} along with the windowed median energy maps at (b) 0–2000 keV, (c) 2000–20 000 keV, (d) 20 000–22 300 keV, (e) 22 300–22 900 keV, and (f) 22 900–23 400 keV.

with 24 MeV carbon ions. Fig. 12 show the damage of the 50 μm mushroom device after irradiation with a ^{12}C ion fluence of approximately 10^8 cm^{-2} to the middle 16 SVs as seen in the median energy maps for different consequent energy windows under a 10 V bias for both the odd and even arrays. It is possible to see the difference in charge collection within the irradiated and nonirradiated SVs. With a 10 V bias applied, the difference between the charge collection within the irradiated SVs is observed at the 22.9–23.4 MeV energy window [Fig. 12(f)] demonstrating that there exists a charge collection deficit of ~1% between the irradiated SVs and nonirradiated SVs. Furthermore, when comparing the CCE of the nonirradiated 50 μm microdosimeter in Fig. 10, it can be seen that after a 10 Mrad(Si) gamma dose and a 10^8 ions/cm^2 fluence of ^{12}C ions, only a ~2% reduction in the CCE is observed.

These results are important for evaluating applications of the SOI microdosimeters for QA in particle therapy and radiation monitoring during space missions. A typical heavy ion therapy center treats approximately 200–500 patients per year. We will consider QA measurements for ^{12}C ion therapy with a microdosimeter, that is placed in the middle of the spread-out brag peak (SOBP) where the average ion energy is about 100 MeV/u. The average carbon ion fluence required for SOI microdosimetry measurements to acquire reasonable statistics in the microdosimetry spectrum based on our experience, is about 10^8 cm^{-2} that corresponds to about 2 Gy absorbed dose in water and about 1.5 Gy(Si). Assuming QA will be carried out in five locations of SOBP with the dose at each point being 2 Gy(Si) for 500 patients per year, this will lead to a TID of 0.5 Mrad(Si)/year and carbon ion fluence of 2.5×10^{11} cm^{-2} that corresponds to a 1 MeV neutron equivalent fluence (ϕ_{eq} (1 MeV)n) of about 3.8×10^{12} cm^{-2}/year using the SR-NIEL-7 calculator [26].

Demonstrated CCE degradation in 50 μm SOI microdosimeter with 10^8 cm^{-2} fluence of 24 MeV carbon ions corresponds to a ϕ_{eq} (1 MeV)n of about 7×10^{11} cm^{-2}. However, this estimated DD corresponds to the entrance of the SV. At a depth of 27 μm at which the maximum DD will be achieved (approximately 280 times higher), corresponds to a ϕ_{eq} (1 MeV)n of about 2×10^{15} cm^{-2}. Average DD in the SV greatly exceeds the expected annual ϕ_{eq} (1 MeV)n of 3.8×10^{12} cm^{-2}. Based on this analysis, the SOI microdosimeter can tolerate TID and DD damage during annual QA for each patient plan for several years without essential degradation.

Suitability of the SOI microdosimeter was evaluated for 1 year Moon mission for unshielded environments. Statistically predicted SPE proton fluences and calculated TID and the DD equivalent fluence (DDEF) of 50 MeV protons in silicon surrounded by a 0.01 mm Al shell was about 0.34 Mrad(Si) and 2.15×10^{12} cm^{-2}, respectively [27]. Effects of GCRs can be neglected. Predicted DDEF corresponding to a ϕ_{eq} (1 MeV)n of 5.68×10^{12} cm^{-2}. Both TID and DD are similar to an expected medical scenario and can be tolerated by developed SOI microdosimeters without any visible damage.

IV. Conclusion

We have investigated the CCE and its degradation versus TID and DD, in a new batch of SOI microdosimeters with a device layer of 10, 20, and 50 μm. Irradiation of the 10 and 20 μm SOI microdosimeters with a 24 MeV carbon ion beam demonstrated negative pulses on the output of the charge sensitive preamplifier in addition to positive pulses from the

SVs. It was confirmed that the origin of the negative pulses in the support wafer is due to the displacement current phenomena. Irradiation of the SOI microdosimeters with 3 Mrad(Si) gammas from a Co-60 source leads to a disappearance of the negative pulse due to the increase in recombination of *e–h* pairs created by the carbon ions in the substrate wafer with minimal changes being observed within the SVs in terms of CCE.

Further irradiation of the SOI microdosimeters with gamma photons of up to 10 Mrad(Si) lead to low energy events being present as a halo between SVs. The origin of the halo is due to the buildup of positive charge in the field oxide and depends on the efficiency of the diffusion charge collection in the device layer.

Irradiation of the 50 μm SOI microdosimeters after a 10 Mrad(Si) gamma dose with 24 MeV carbon ions with a fluence of approximately 10^8 ^{12}C ions/cm^2 (equaling a $\sim 7 \times 10^{11}$ 1 MeV neutron equivalent fluence) does not lead to a CCE deficit of more than 2% for a 10 V bias when compared to a virgin device. Such radiation hardness of the SOI microdosimeters makes them attractive for QA in particle therapy and Lunar space missions.

The following recommendations can be concluded from these studies for further optimization of SOI microdosimeters: 1) SOI microdosimeters should be fabricated with the lowest possible resistivity of the support wafer (<0.01 Ωcm) and a BOX thickness larger than 1 μm and 2) high concentration p+ spray between the SVs should be deposited on the device layer to mitigate the effect of buildup charge in the field oxide.

ACKNOWLEDGMENT

The authors would like to thank the help provided by the Australian Government Research Training Program Scholarship and the Post Graduate Research Award (PGRA) from the Australian Institute of Nuclear Science and Engineering (AINSE).

REFERENCES

[1] D. Wagenaar et al., "Validation of linear energy transfer computed in a Monte Carlo dose engine of a commercial treatment planning system," *Phys. Med. Biol.*, vol. 65, no. 2, Jan. 2020, Art. no. 025006.

[2] S. Peracchi et al., "Radiation shielding evaluation of spacecraft walls against heavy ions using microdosimetry," *IEEE Trans. Nucl. Sci.*, vol. 68, no. 5, pp. 897–905, May 2021.

[3] V. A. Pan et al., "Application of an SOI microdosimeter for monitoring of neutrons in various mixed radiation field environments," *IEEE Trans. Nucl. Sci.*, vol. 69, no. 3, pp. 491–500, Mar. 2022.

[4] G. Lindström, "Radiation damage in silicon detectors," *Nucl. Instrum. Methods Phys. Res. A, Accel. Spectrom. Detect. Assoc. Equip.*, vol. 512, nos. 1–2, pp. 30–43, Oct. 2003.

[5] D. M. Fleetwood, "Total-ionizing-dose effects, border traps, and 1/f noise in emerging MOS technologies," *IEEE Trans. Nucl. Sci.*, vol. 67, no. 7, pp. 1216–1240, Jul. 2020.

[6] J. R. Srour and J. W. Palko, "Displacement damage effects in irradiated semiconductor devices," *IEEE Trans. Nucl. Sci.*, vol. 60, no. 3, pp. 1740–1766, Jun. 2013.

[7] P. V. Dressendorfer, *Basic Mechanisms for the New Millennium*. Kansas City, MI USA: IEEE NSREC Short Course, 1999.

[8] P. D. Bradley, A. B. Rosenfeld, and M. Zaider, "Solid state microdosimetry," *Nucl. Instrum. Meth. Phys. Res. B, Beam Interact. Mater. At.*, vol. 184, nos. 1–2, pp. 135–157, 2001.

[9] G. D. Badhwar, "Shuttle radiation dose measurements in the international space station Orbits," *Radiat. Res.*, vol. 157, no. 1, pp. 69–75, Jan. 2002.

[10] L. T. Tran et al., "The relative biological effectiveness for carbon, nitrogen, and oxygen ion beams using passive and scanning techniques evaluated with fully 3D silicon microdosimeters," *Med. Phys.*, vol. 45, no. 5, pp. 2299–2308, May 2018.

[11] A. Kok et al., "Fabrication and first characterization of silicon-based full 3-D microdosimeters," *IEEE Trans. Nucl. Sci.*, vol. 67, no. 12, pp. 2490–2500, Dec. 2020.

[12] A. Ziebell et al., "A cylindrical silicon-on-insulator microdosimeter: Charge collection characteristics," *IEEE Trans. Nucl. Sci.*, vol. 55, no. 6, pp. 3414–3420, Dec. 2008.

[13] S. Peracchi et al., "Modelling of the silicon-on-insulator microdosimeter response within the international space station for astronauts' radiation protection," *Radiat. Meas.*, vol. 128, Sep. 2019, Art. no. 106182.

[14] S. Peracchi et al., "Modelling of protons spectra encountered in space using medical accelerator and its microdosimetric characterization," *Adv. Space Res.*, vol. 67, no. 8, pp. 2534–2543, Apr. 2021.

[15] S. Peracchi et al., "A solid-state microdosimeter for dose and radiation quality monitoring for astronauts in space," *IEEE Trans. Nucl. Sci.*, vol. 67, no. 1, pp. 169–174, Jan. 2020.

[16] V. A. Pan et al., "Characterization of a novel large area microdosimeter system for low dose rate radiation environments," *Nucl. Instrum. Methods Phys. Res. A, Accel. Spectrom. Detect. Assoc. Equip.*, vol. 1002, Jun. 2021, Art. no. 165238.

[17] L. T. Tran et al., "Silicon 3D microdosimeters for advanced quality assurance in particle therapy," *Appl. Sci.*, vol. 12, no. 1, p. 328, Dec. 2021.

[18] L. T. Tran et al., "Characterization of proton pencil beam scanning and passive beam using a high spatial resolution solid-state microdosimeter," *Med. Phys.*, vol. 44, no. 11, pp. 6085–6095, Nov. 2017.

[19] D. Sakata et al., "Microdosimetric investigation for multi-ion therapy by means of silicon on insulator (SOI) microdosimeter," *Phys. Med. Biol.*, vol. 67, no. 21, Oct. 2022, Art. no. 215010.

[20] B. James et al., "SOI thin microdosimeters for high LET single-event upset studies in Fe, O, Xe, and cocktail ion beam fields," *IEEE Trans. Nucl. Sci.*, vol. 67, no. 1, pp. 146–153, Jan. 2020.

[21] C. Fleta et al., "3D cylindrical silicon microdosimeters: Fabrication, simulation and charge collection study," *J. Instrum.*, vol. 10, no. 10, Oct. 2015, Art. no. P10001.

[22] C. Guardiola, C. Fleta, D. Quirion, G. Pellegrini, and F. Gómez, "Silicon 3D microdetectors for microdosimetry in hadron therapy," *Micromachines*, vol. 11, no. 12, p. 1053, Nov. 2020.

[23] J. Ziegler. *SRIM*. Accessed: Oct. 2022. [Online]. Available: http://www.srim.org/

[24] J. R. Schwank et al., "Charge collection in SOI capacitors and circuits and its effect on SEU hardness," *IEEE Trans. Nucl. Sci.*, vol. 49, no. 6, pp. 2937–2947, Dec. 2002.

[25] H. Tsujii and T. Kamada, "A review of update clinical results of carbon ion radiotherapy," *Japanese J. Clin. Oncol.*, vol. 42, no. 8, pp. 670–685, Aug. 2012.

[26] M. J. Boschini, *SR-NIEL-7 Calculator: Screened Relativistic (SR) Treatment for Calculating the Displacement Damage and Nuclear Stopping Powers for Electrons, Protons, Light- and Heavy-Ions in Materials (Version 9.0)*. INFN Sez. Milano-Bicocca, Italy, 2014. Accessed: Nov. 2022. [Online]. Available: http://www.sr-niel.org/

[27] *Crossprogram Design Specification for Natural Environments (DSNE)*, document SLSSPEC-159 Revision D, National Aeronautics and Space Administration (NASA), Nov. 2015.